



Additive manufacturing by digital light processing: a review

Rajat Chaudhary¹ · Paride Fabbri² · Enrico Leoni² · Francesca Mazzanti² · Raziye Akbari¹ · Carlo Antonini¹

Received: 9 March 2022 / Accepted: 30 July 2022 / Published online: 25 August 2022
© The Author(s) 2022

Abstract

Additive manufacturing is a layer-by-layer strategy enabling the advanced design and fabrication of complex 3D objects and structures, overcoming geometry limitations and reducing waste production compared to conventional technologies. Among various additive manufacturing technologies, digital light processing (DLP), is an additive manufacturing technology used to print photopolymer parts, using a projected light source to cure an entire layer at once. Initially developed for pure resins, recent advances have demonstrated the potential of DLP in the polymerization of ceramic and metal-loaded suspensions, enabling the fabrication of ceramic and metal components after proper debinding and sintering. Such flexibility increases the potential of DLP for different applications, ranging from dental implants and bone scaffolds to smart biomaterials for soft robotics, smart wearables, and microfluidic devices. The review provides an overview of DLP technology and its recent advances; specifically, the review covers the photopolymer properties, the ceramic and metallic feedstock preparation, and the light-matter interaction mechanism underpinning the printing and post-processing steps. Finally, a description of the current application is provided and complemented with future perspectives.

Keywords Digital light processing · Stereolithography · Vat polymerization · Dynamic mask stereolithography · Suspensions

1 Introduction

Additive manufacturing, rapid prototyping, rapid manufacturing, layer-oriented manufacturing, digital fabrication, 3D printing [1], and many more terms have been introduced after the patent filed by Chuck Hull in 1984 [2] before standardization in ISO/ASTM 52900: 2015 (Additive manufacturing—General Principles—Terminology). At present, the term additive manufacturing (AM) is more common in the scientific and technical communities, whereas 3D printing is usually preferred in communications to the general public. In a nutshell, AM reverses the conventional approach of subtractive fabrication techniques: it is based on layer-upon-layer fabrication of an object, starting with liquid or solid powder as a raw material to form a three-dimensional

(3D) object from stacking of two-dimensional (2D) layers. Within the framework of the fourth industrial revolution, also referred to as Industry 4.0 [3], AM is a part of the larger plan to integrate digital technology and Internet of Things (IoT) with conventional technologies [4]. This integration leads to the reduction of space needed for production, irrespective of the output mass, and can help to reduce the efforts into setting up a conventional manufacturing unit by facilitating customization. One of the most significant advantages of AM is the almost constant manufacturing cost, which is independent of the production scale and, to some extent, the product shape complexity [5] (Fig. 1a). Minimal production of wastes makes this technology environmental-friendly [6] and provides an advantage towards sustainable manufacturing compared to traditional manufacturing methods. These features have attracted various manufacturing sectors [7], such as biomedical/dental [8–10], automobile [11], aviation [12], and construction [13], from the early stages of AM development. Many more sectors are adopting AM, making the manufacturing process economically affordable and environmentally sustainable (Fig. 1b). As a result, AM technology has gained remarkable popularity in

✉ Carlo Antonini
carlo.antonini@unimib.it

¹ Department of Materials Science, University of Milano-Bicocca, Milan, Italy

² Laboratorio Tecnologia Dei Materiali Di Faenza, ENEA, Faenza, Italy

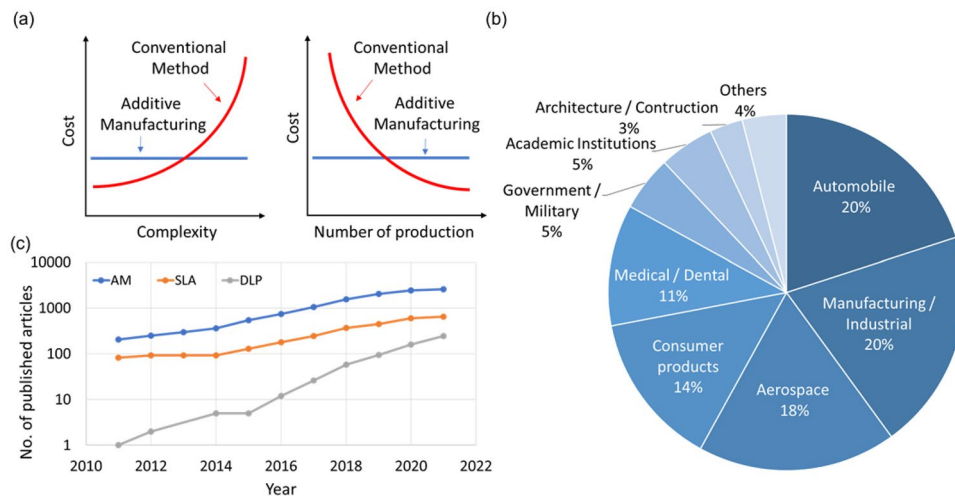


Fig. 1 **a** Comparison of additive manufacturing and conventional manufacturing methods in cost, complexity, and the number of productions. **b** Distribution of AM revenues from different sectors (Source: Canada's Additive Manufacturing Ecosystem, ICTC; Wholers 2019). **c** Statistics related to AM, extracted from Scopus, show an increase in articles published from 2011 to 2021. The following keywords were used to extract results: for "AM"- {Selective laser sintering} OR {selective laser melting} OR {laser engineered net

shaping} OR {prometal} OR {3DP binder jetting} OR {laminated object manufacturing} OR {fused deposition modelling} OR {polyjet technology} OR {stereolithography} OR {vat polymerization}; for "SLA"- {stereolithography} OR {vat polymerization}; for "DLP"- ("Digital light processing") AND ("Additive Manufacturing") OR ("3D Printing"). The keywords were searched within TITLE-ABS-KEY. (Query performed on: 20th January 2022)

the last decade. The industrial potential is also reflected by the steady and exponential rise in the number of research articles (Fig. 1c), which have focused on the development of new technologies improving AM by achieving faster and cost-effective processes, and materials with enhanced properties (mechanical, finishing, etc.).

In recent years, a new variety of materials and AM technologies [14, 15], including friction-based [16, 17], has been developed for various applications [18]. In this review, we have focused specifically on the emerging vat photopolymerization-based digital light processing (DLP) technology for the manufacturing of various materials, including not only photosensitive resins but also ceramic materials, metals, and composites, producing high-resolution geometries for myriad applications, which has been experiencing rapid growth since 2016 (Fig. 1c).

The objective of this review is to highlight DLP novelties and peculiarities in contrast to other AM technologies, including: (a) high-resolution DLP source, a simple and inexpensive device that nonetheless allows reaching printing resolution of few microns in the printing plane; (b) mask projection-based approach, which ensures a fast printing compared to multistep mask-based processes or laser-based manufacturing technologies, requiring time-consuming scanning in XY plane; (c) availability of a variety of materials offering DLP a potential of manufacturing of functional and nonfunctional parts; (d) possibility of biomaterial printing, due to low-power DLP source; and (e) low cost and user-friendliness of printers makes it available even

to inexperienced users. This paper covers various aspects of the DLP printing process including material preparation and advancements and provides insight into light-matter interaction during printing.

The review is structured as follows. Section 2 provides a general overview of the AM and briefly compares the main AM approaches. Section 3 presents the DLP technology and its advances in detail and describes its peculiarities. Sections 4 and 5 are dedicated to materials that can be manufactured by DLP, including resins and particle-loaded slurries. Section 6 provides the theoretical framework of light-matter interaction that can be used to understand, develop, and optimize the manufacturing process. Sections 7 and 8 are devoted to post-processing and applications, respectively. Final remarks and future perspectives are presented in the conclusion section.

2 Additive manufacturing

Additive manufacturing of a 3D object can be divided into three major steps: (i) designing, (ii) printing, and (iii) post-processing [19]. In the designing step, the desired 3D shape is created using CAD (computer automated design) software (Fig. 2a), such as TinkerCAD, Fusion 360, SOLIDWORKS, AutoCAD, etc. In a classic manufacturing process, the designed geometry is converted into STL (Standard Tessellation Language) format [20] and sliced into 2D images (layers) by slicing software (Fig. 2b). The output file from

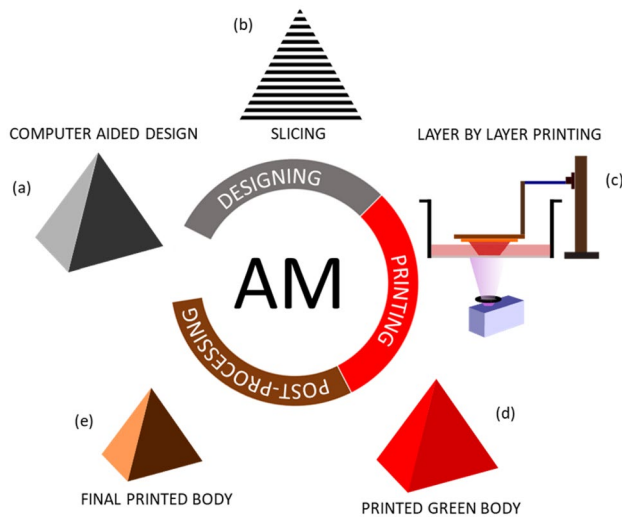


Fig. 2 Step-by-step manufacturing process in AM. Designing step consists of CAD modeling and slicing of a 3D object (a, b). These sliced layers are printed one layer after the other in the printing process (c). The printed body in green form (d) is then subjected to post-processing before emerging out as a final printed body (e)

the slicing software contains the geometrical information related to the sliced layers. Printing parameters such as exposure time, which depend on the technique and the specific process, are typically defined in the printer software before printing. Currently, 3D printers, based on different manufacturing technologies use G-codes generated by the printer software and are compatible with different formats of 3D files. These G-codes contain all the information required for printing, including printer movements, sliced images, exposure time, temperature, etc. During printing (second step), 2D slices (layers) are printed one after the other, until the final object emerges on the build head as a compact stack of layers (Fig. 2c). This manufactured object, also called ‘green body’ (Fig. 2d) at this stage, is then removed from the build head and subjected to post-processing (third step). Post-processing is required to remove the excess raw material or impart the final finishing (Fig. 2e) which may depend on the specific AM technology, the material used, and the final application for produced parts.

A variety of AM technologies have evolved in the last forty years, and the categorization is not unique. Process- [21] and material-based [22] classifications are more frequently used. A brief description of the most widely used manufacturing technologies [23] is provided here while comparing their key properties (Table 1).

3 Digital light processing

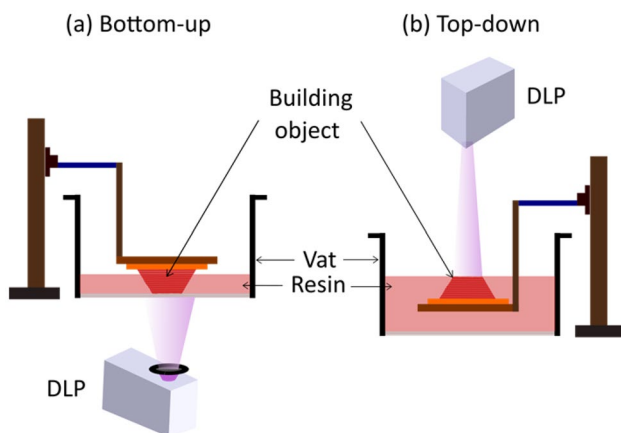
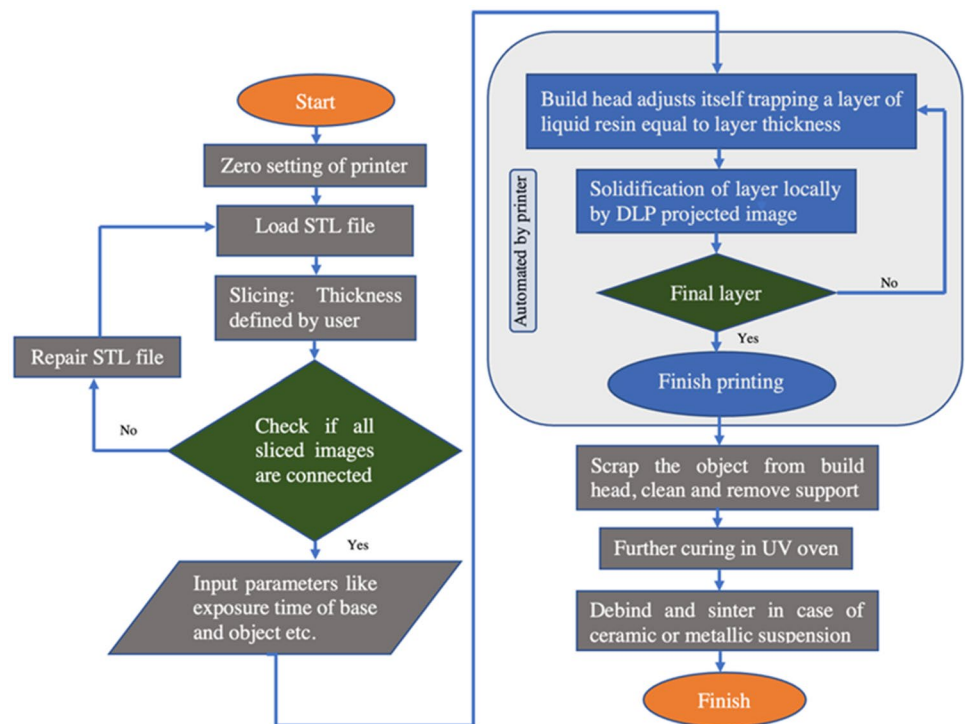
DLP is named after the digital light projector [45], based on digital micro-mirror device (DMD) technology [46]. The photosensitive resin is polymerized locally and forms a stack of layers by a back-to-back projection of images of 2D layers from a DLP source. These images are an ensemble of light and dark pixels created by micron-sized mirrors on DMD, which determine the XY-plane resolution of the polymerized layer. The technology comes under the category of the vat polymerization process, along with stereolithography. It shares the same fundamental steps of manufacturing as other AM technologies, i.e., designing, printing, and post-processing. A brief representation of the complete DLP process is illustrated in the flowchart in Fig. 3. Preprinting steps may change, based on the specific CAD and slicing software. For example, some slicing software can generate support structures, or can repair critical issues in the .stl file, such as holes or intersections.

In principle, the printing process is similar for all DLP-based printers. However, geometric configurations may differ. Two main geometric configurations [47] are usually adopted in DLP: bottom-up and top-down. In the bottom-up configuration (Fig. 4a), the build head is dipped in the resin container (vat); the immersion height (i.e., the distance from the head to the vat base) is equal to the desired layer thickness. The transparent bottom of the vat allows the UV light to pass through and project the image onto the thin layer of liquid resin, trapped between the vat base and the build head. The trapped liquid resin layer is polymerized and remains attached to the build head after a defined exposure time. The upward movement of the build head helps in the separation of the polymerized layer from the vat base. As the building head moves up, the vat base is recoated with a fresh liquid layer of unpolymerized resin. Differently, in the top-down configuration (Fig. 4b), the DLP source is mounted at the top of the vat, and the build head is completely immersed inside the resin container. The build head depth is kept equal to the desired layer thickness. This thin layer over the build head is then cured by the DLP source mounted above the vat. After curing, the build head with adhered first layer shifts down inside the container to a distance equal to layer thickness. A recoating blade is used to fill the void space with a fresh layer of resin.

Each configuration presents its advantages. The bottom-up configuration requires less fresh resin in the vat and can print small objects with less resin in the container. Vacuum

Table 1 Comparison of different AM technologies

| AM Technology | Process | Power Source | Material | Accuracy and Finish | Post-processing | Application | References |
|---------------|--------------------------|---------------------------------|---|--|--|--|------------|
| SLS | Powder bed fusion | Low power laser | Polymeric, Ceramic, Metal powder | Not very accurate/Standard Finish | Sintering, infiltration | Prototypes, casting | [24, 25] |
| SLM | | High power laser | Metal powder | Surface quality is limited by the size of particles | Infiltration, surface finish | Tools, functional Parts | [26, 27] |
| EBM | | Electron beam | Metal powder | Low surface quality but with high density | Infiltration, surface finish | Tools, functional Parts | [28, 29] |
| LENS | Direct energy deposition | Laser | Metal powder | Poor surface quality | Cleaning | Biomedical: bone implants and scaffolds | [30, 31] |
| 3DP | Binder jetting | Chemical reaction of the binder | Liquid binder, starch-based powder, ceramic | Low z-resolution | No chemical post-processing, polishing for smooth surface | Prototypes, casting | [32, 33] |
| LOM | Sheet lamination | Laser or blade | Paper, plastic, metal, ceramic, fiber | Less dimensional accuracy, delamination is common | Polishing, Painting | Prototypes, non-functional parts | [34, 35] |
| FDM | Material extrusion | Heating element for filament | Plastic, ceramics, composites | Low z-resolution | Finishing for surface smoothness | Modeling, prototyping | [36–38] |
| POLYJET | Inkjet printing | UV source | Photopolymers | High resolution, different materials, low mechanical strength | Removal of the support structure | For prototypes latest research claims end to use as well | [39, 40] |
| SLA/DLP | Vat polymerization | UV Laser (SLA)/DLP | Photopolymer, ceramic/metal powder (optional) | One of the most accurate printing processes/Excellent surface finish | Removal of the support structure. Debinding and sintering (for metal and ceramics) | Prototypes, casting, end-to-use parts | [41–44] |

Fig. 3 Schematic flow diagram of a DLP printing process**Fig. 4** Two different geometries are used in DLP-based printing technology. **a** Bottom-up: the object is built inverted on the build head by polymerizing the layers exposed from the bottom of the vat. **b** Top-down: the object is manufactured on the build head by polymerizing the layers exposed from the top of the vat

developed with the upward movement of the build head facilitates the recoating process even for the viscous resins. However, the separation of polymerized layers from vat base media is a critical step during the printing process. Flexible films [48], coated films [49, 50], and separation movements [51, 52] have been introduced to overcome the adherence of polymerized film with the vat base. Differently, in the top-down configuration, a higher amount of less viscous resin is required. This aids the adjustment of the build head

inside the vat with a resin layer on the top. However, printers equipped with recoater/scrapper make the coating easier even for highly viscous resins or resin filled with solid particles. An advantage of the top-down configuration is that there are no issues with adherence between layer and vat base media, as the resin is polymerized at the free surface, in contact with air. However, the contact of environmental oxygen to the resin surface may inhibit the polymerization on the projection site. Consequently, both configurations have pros and cons, and commercial printers on the market exploit both configurations.

Several advancements in the technology have been introduced recently to overcome the abovementioned limitations, including single material restriction inside vat in both configurations. Multi-vat DLP systems or material swaps enabled the fabrication of multi-material mechanical, electrical and bio-functional components [43, 53, 54] (Fig. 5a). Another approach for manufacturing multi-materials is the integration of two different manufacturing technologies. Peng et al. demonstrated the printing of multifunctional structures and devices using an integrated DLP and direct ink writing (DLW) system [55] (Fig. 5b), whereas Nguyen et al. presented the integration of DLP with binder jet printing (BJP) in their research for metal components manufacturing [56].

Other methods have been implemented in DLP for improving the process. The time-consuming and critical post-polymerization detachment from the vat base in bottom-up DLP was eliminated by Continuous Liquid Interface

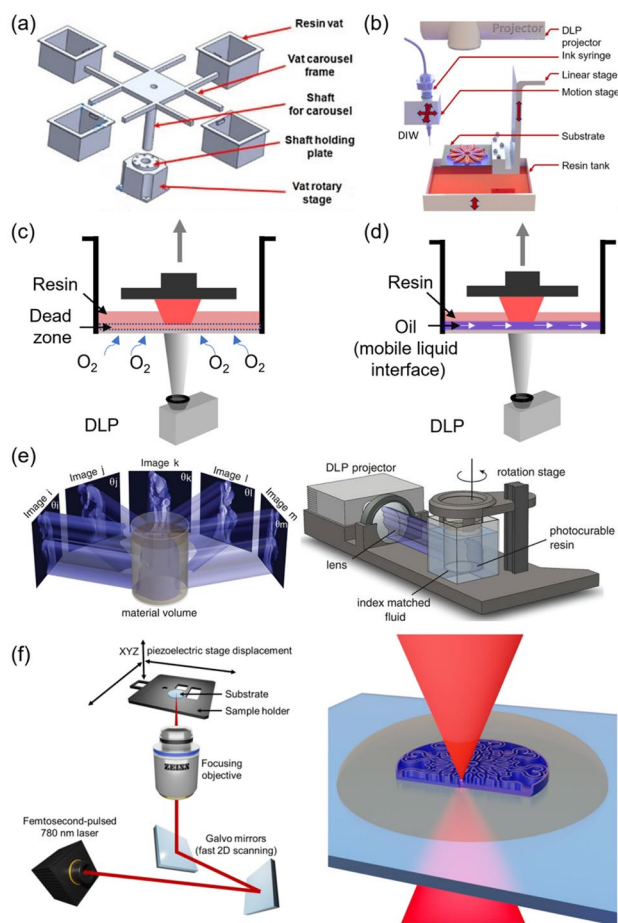


Fig. 5 Advances in DLP and similar vat polymerization technologies: **a** multi-vat system for switching photopolymers for multi-material printing (adapted and reprinted from ref. [62] with permission from Elsevier. **b** Multi-material printing with hybrid printing technology using DLP and DIW (adapted and reprinted from ref. [55] with permission from Elsevier). **c** Schematic of CLIP method. **d** Schematic of HARP method. **e** Vat polymerization-based volumetric additive manufacturing (adapted and reprinted from ref. [59] with permission from Science). **f** Two-photon polymerization (adapted and reprinted from ref. [61] licensed under a Creative Commons license, CC BY 4.0)

Production (CLIP) method (Fig. 5c): Janaszewicz et al. introduced an oxygen preamble window, which generates a continuous liquid interface, also called “dead zone”, by inhibiting polymerization between the polymerized resin and the vat base [57]. The method not only facilitates an increase in manufacturing speed but also limits staircase effects in manufactured objects. In another similar approach, high-area rapid printing (HARP, see Fig. 5d), this dead zone is replaced by mobile immiscible fluorinated oil at the interface, which reduced the adhesion between polymerized resin and the vat base [58]. Tomographic volumetric additive manufacturing (Fig. 5e) is another extension of vat polymerization-based technologies after SLA and DLP, where liquid photopolymer is selectively polymerized by projecting

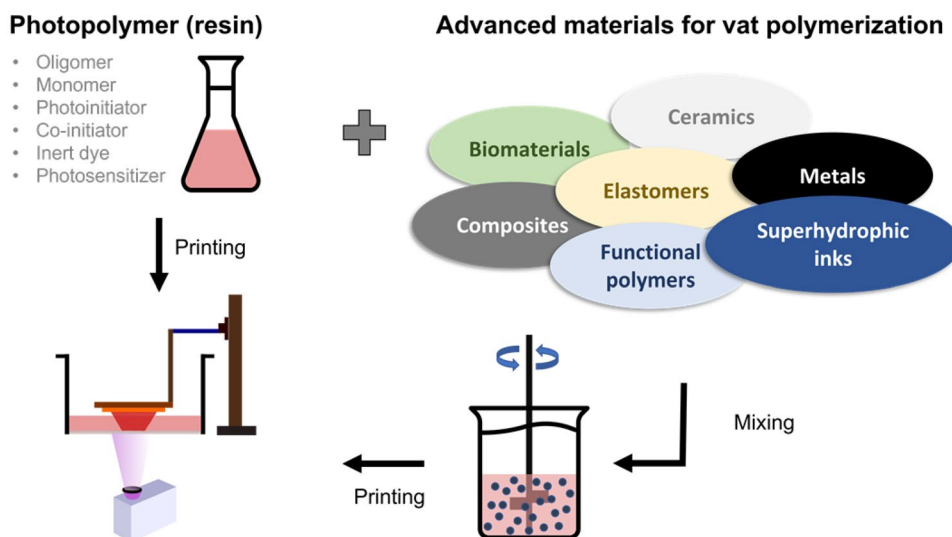
two-dimensional images inside the material volume [59]. Based on the principle of computed tomography (CT), collective energies of propagated images at multiple angles through the material help in getting desired geometry in a shorter time than layer-by-layer methods. Similar to volumetric additive manufacturing, photopolymer is cured freely inside vat using a laser beam in two-photon polymerization (2PP) technology [60] (Fig. 5f). The minimum identity of freely cured photopolymers (called “voxel”, which stands for “volumetric pixel”) allows manufacturing of micro-objects with nanometric features [61].

4 Materials: from pure resins to suspensions

A simplified system of photopolymer (resin) [63] contains oligomers, monomers (mono- or poly-functional), and a small amount of photoinitiator (PI). Oligomers are long chains of molecules that provide the backbone to the photoinitiating system, while monomers are utilized as diluting agents. Resin exposure to the light source activates the PI, which generates reactive species, free radicals, or reactive ions. These species react with oligomers and monomers, enabling the formation of long chains leading to photopolymerization [64, 65]. Monomers and oligomers alone are not able to produce enough reactive species for polymerization. Hence, a small amount of PI is needed for initiating the process [66]. To increase the PI yield, more complex photoinitiating systems are developed, including co-initiator, inert dyes, photosensitizers, etc. [67]. Furthermore, the high reactivity of resins to radiation allows the addition of fillers (ceramic or metal) to the base resin formulation to form a suspension [42] (Fig. 6). In these systems, photopolymerized resin provides a matrix to solid particles. Later, the organic part is removed in the post-processing step called debinding. The remaining porous solid structure is then sintered at an optimized temperature creating a dense solid part.

The proportion of the components inside photopolymer affects the printing process in several ways. Specifically, oligomers with a small number of repeated units have a higher molecular weight than monomers. A high proportion of oligomers increases the printed object mechanical strength, but also increases the liquid photopolymer viscosity, decreasing the flowability and hindering the recoating process in the vat. Conversely, increasing the monomer percentage reduces liquid viscosity, but increases the polymerization time to achieve similar mechanical properties. As such, the proportion of oligomers and monomers is essential to tune the resin viscosity, the exposure time for polymerization, and the final properties of the printed object [68]. The viscosity of the photoinitiating system also depends on fillers, which is detailed in Sect. 5. In

Fig. 6 Schematic illustrating material composition for vat polymerization process, which can be either a pure resin or advanced material, such as ceramic or metal suspensions, which can be added and mixed with the resin before printing



general, the steps for polymerization are the same for all the photopolymers while interacting with the radiation, but the mechanism is different based on the photoinitiating system which is detailed in the next sections.

4.1 Photoinitiating (PI) systems

Photopolymers are categorized based on photoinitiating reactions: (i) free radical and (ii) ionic-based [66]. These systems differ by the produced reactive species by PI, radicals, and reactive ions, as they are exposed to a light source, starting chain reactions leading to photopolymerization. Both free radical and ionic-based processes consist of three steps, schematically represented in Fig. 7: (i) initiation, (ii) propagation, and (iii) termination. Initiation starts with the absorption of UV radiation by PI generating the reactive species. These species react with oligomers and monomers, promoting the formation of long chains during the propagation step. The reaction terminates

either of the three causes, recombination, disproportionation, or occlusion [69].

Free radicals can crosslink acrylate, styrene, and thiolene-based monomers, to form a long chain responsible for free radical polymerization. This process is fast and terminates in the absence of radiation [70]. Differently, ionic species induce ionic polymerization of another category of monomers such as ketones, aldehydes, heterocyclics, etc., which are not polymerized by free radicals [71]. Cationic polymerization is more widely used in the latter polymerization system, while it needs more exposure time than radical polymerization and continues even after the removal of the light source.

4.1.1 Free radical system

In these photoinitiating systems, free radicals are generated from the photoinitiator after exposure to light radiation [70]. Acrylates (di- or multifunctional) (highly reactive) are the main choice for these kinds of formulations. Unimolecular

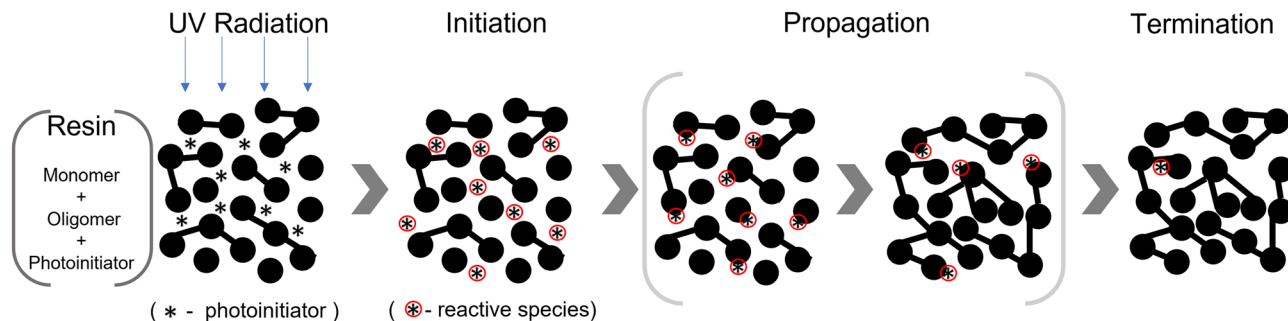


Fig. 7 Schematic of the polymerization process of a photosensitive resin. The photoinitiator (black star) generates reactive species (star in a red circle) during the initiation process, as soon as the photosensitive resin is irradiated by UV light. The reactive species react with

monomers and oligomers and start photopolymerization in the propagation step, followed by the termination step resulting in the polymerization of the liquid photopolymer

4.1.2 Ionic system

In ionic photoinitiating systems, polymerization is promoted by anions in anionic systems and by cations in cationic systems [71]. In anionic polymerization, a nucleophilic group or an electron is transferred to a monomer by anionic PI to initiate photopolymerization. Anionic photoinitiating systems are more challenging to control than radical-based systems; therefore, they are usually considered a secondary option. Cationic photoinitiating systems are more widely used and well-explored for the vat polymerization process. Thus, this review is focused more on cationic polymerization in ionic-based PI, along with free radical polymerization.

Onium salts, diazonium salts, and organometallic complexes are the main categories of a cationic PI system [73]. Figure 8 depicts the generation of reactive species, i.e., cations from onium salts in three ways: (i) direct photolysis of PI, (ii) sensitized photolysis of PI, and (iii) free radical mediation upon irradiation with light source followed by initiation, propagation, and termination step. In direct photolysis, a radical cation and a proton, generated after photolysis of the onium salt, react with the monomer during initiation. In the mixture of PI and photosensitizer (PS), initiation can start in three possible ways: (i) radical cation (oxidized PS by onium salt), (ii) cation generated by oxidized PS, and (iii) radical from onium salt, and proton. In the free radical promoted system, the reactive species are generated by the oxidation of carbon-centered free radical by the onium salts. Unlike the free radical systems, nucleophilic impurities of the PI system terminate the chain photopolymerization process in cationic systems [74].

4.2 Oligomers and monomers

Oligomers and monomers represent the largest component in photosensitive resins. These molecules crosslink together in a chain process, creating a crosslinked polymer after reacting with UV activated photoinitiator. Generally, acrylates, mono- and poly-functional, with olefinic double bonds, are chosen in free radical systems. Compounds like epoxides and vinyl ether, which do not polymerize with free radical photoinitiators, are polymerized with cationic-based photoinitiators; n-butyl acrylates (BA), 1,6-hexanediol diacrylate (HDDA), poly (ethylene glycol) diacrylate (PEGDA), pentaerythritol triacrylate (PETA), 1,4-cyclohexanedimethanol divinyl ether (CHDMDE) are a few examples of acrylate-based monomers commonly used. 3,4 epoxy-cyclohexanemethyl 3, 4 epoxy-cyclohexylcarboxylate (EPOX), diglycidyl ether (DGEBA), 1,4-cyclohexane dimethanol divinyl ether (CDVE) [75] works for cationic based polymerization process [57].

Both free radical and ionic photopolymerization have their advantages and disadvantages [76]. In free radical photopolymerization, acrylates are more reactive and polymerize rapidly, but may experience deformations, such as shrinkage and curls, in polymerized parts; conversely, in ionic photopolymerization, epoxy-based resins cure slowly and even after the radiation stops, resulting in lower risks for defects. Epoxy-based resins possess less odor and toxic compounds in comparison with acrylates. Photopolymerization is not affected by environmental oxygen in ionic polymerization as in radical polymerization. Currently, a mixture of acrylate-based and epoxy-based resins are used to formulate optimized resins. However, a large number of acrylate-based resins are available compared to epoxy-based alternatives.

5 Resin suspension

During the initial development of stereolithography, the technology was only limited to liquid photopolymers as raw material. The need to produce solid parts with high mechanical properties and functionalities motivated the researchers to incorporate micro and nano-size fillers inside the liquid photopolymer to cover a variety of applications [77, 78]. Ceramic powders were one of the first choices as fillers due to their chemical inactivity with the organic resin, to produce non-functional prototypes.

Moreover, vat polymerization is currently studied as a new forming technique to produce components made of different materials (e.g., ceramics and metals) for many applications, by tuning material mechanical strength, electrical conductivity, biocompatibility, etc. Therefore, the following sections are mainly focused on ceramic-filled photopolymers, as well as the more recent development of printing metal parts using metal powder-filled photopolymers.

5.1 Ceramic feedstock

Vat polymerization can be considered a promising process for the net-shape forming of complex ceramic components. Compared to gel-casting and injection molding, net-shape techniques are already mature at an industrial level, as vat polymerization does not require expensive multi-part molds for casting or injection, and allows the realization of complex geometries [79].

DLP technology allows the manufacturing of monolithic ceramic components, either porous or dense. Two types of ceramic feedstock can be distinguished for vat polymerization: photopolymerized suspensions and photopolymerized preceramic resins. The first type of resins provides a heterogeneous dispersion of solid particles in a mixture of liquid monomers, whereas the latter type is a homogeneous

mixture of resins in which the ceramic precursor is present. After printing, the object requires two thermal treatments: debinding (to remove the polymer matrix) and sintering (for material consolidation).

5.1.1 Photopolymerizable suspensions

In this case, the ceramic feedstock is a suspension in which the photopolymerized organic matrix and the photoinitiator are mixed with the ceramic powder. This approach of fabricating ceramic parts with photopolymerizable suspension has been developed almost in parallel with the stereolithography technique [80–82], but optimizing a ceramic suspension is still a challenge. First, the ceramic filler plays an active role within the suspension, interfering with the penetration of radiation. The main reason is the scattering that is generated by the mismatch of refractive indexes between the ceramic powder and monomer; moreover, scattering depends on the solid content and the size of the powder [79, 83, 84]. For this reason, it is easier to control photopolymerization with fillers having a refractive index similar to that of the resin. The optimization of ceramic feedstocks containing materials with a high refractive index such as ZrO_2 and SiC powders (Table 2) is still an interesting challenge.

Another aspect to be considered in the preparation of ceramic suspensions for vat polymerization is viscosity. To avoid crack formation in the ceramic components during the debinding phase and to limit the sintering shrinkage, it is important to maximize the solid content of the ceramic suspension, usually $> 40\%vol$ [81, 84, 85]. However, the increase of the solid content significantly affects the rheological behavior, from a typical Newtonian behavior observed for pure resins to a shear-thinning behavior for concentrated suspensions [85, 86]. On one hand, high viscosity or gel-like behavior makes the suspension more stable, decreasing the sedimentation effect during the photopolymerization process, on the other hand, it reduces the flowability. Indeed, the

suspension should have a sufficiently low viscosity, so that a fresh liquid layer can be restored after printing each layer. This aspect is also a function of the device used for printing: the film formation occurs naturally due to gravity, due to the tilting or oscillating movement of the vat (in a bottom-up geometry/configuration, see Fig. 4, or following the passage of a recoating device/scrapper (in a top-down configuration). The suitable viscosity for printing is generally less than $20 Pa\cdot s$ (at a shear rate of $100 s^{-1}$ at $25\text{ }^\circ C$) for devices equipped with recoating devices/scrapers [87] and less than $3 Pa\cdot s$ [88] with printers without recoating device/scrapper. Reactive diluents (often monofunctional monomers) or inert diluents (not participating in the photopolymerization reaction) in the formulation of photopolymerizing suspensions can be used to reduce viscosity [89, 90].

The preparation of a well-dispersed ceramic suspension begins with the mixing of the components in the liquid phase: monomers and oligomers. Ceramic powder is commonly incorporated directly into the pre-mix (mixing of monomers and oligomers, dispersing, etc.) using grinding/mixing systems capable of breaking down agglomerates: ball milling and planetary milling are the most common methods [91–93]. Generally, the addition of the photoinitiator occurs only at the end of this phase to prevent unwanted reactions catalyzed by the temperature of the grinding process.

To obtain a high solid content suspension, which, nonetheless, has good fluidity, it is often necessary to add a suitable dispersant to the organic powder-matrix system [88, 94, 95]. Since the suspensions are colloidal, the interaction between the ceramic particles is relevant and depends not only on the viscosity but also on stability against sedimentation. Dispersant agents are commonly used to increase the repulsion force between particles and limit their agglomeration.

In some studies, the photopolymerizing suspension preparation is obtained in two steps [96–98]. In the first step, the ceramic powder is disaggregated into a highly diluted suspension, in which the dispersant is dissolved; at the end of

Table 2 Physical properties of the reactants and fillers used (data from Ref. [83])

| Product | Density | η (mPa s) at $25\text{ }^\circ C$ | Specific area ($m^2 g^{-1}$) | d_{50} (μm) | Refractive index n (365 nm) |
|-----------|---------|--|--------------------------------|----------------------|-------------------------------|
| PEAAM | 1.15 | 70 | – | – | 1.488 |
| HDDA | 1.02 | 7 | – | – | 1.456 |
| Al_2O_3 | 3.97 | – | 1.52 | 2.3 | 1.787 |
| Al_2O_3 | 3.97 | – | 2.41 | 1.4 | 1.787 |
| Al_2O_3 | 3.97 | – | 5.74 | 0.5 | 1.787 |
| SiO_2 | 2.26 | – | 5.31 | 2.25 | 1.564 |
| ZrO_2 | 5.92 | – | 4.48 | 0.65 | 2.249 |
| SiC | 3.38 | – | 0.60 | 12.25 | 2.553 |

d_{50} is the value of the particle diameter at 50% in the cumulative distribution

the process, the solvent (water or ethanol) is removed by using a rotational evaporator or by separation after centrifuge [99]. The obtained ceramic powder is dried and sifted then added to the resin mixture. Wang et al. reported that dispersant adsorption is more effective, and, in particular, the adsorption phase is not affected by competition by the mixture of monomers [96]. Moreover, with the same solid content, the viscosity obtained by two steps is less than that of the one-step preparation process [97].

In the preparation of photopolymerizing resins, the use of nanometric silica is also possible to manufacture transparent glass components. The presence of monomers, able to create a solvation layer on silica particles, in the resin makes it possible to obtain concentrated suspensions while maintaining low viscosity without additional dispersing additives [100, 101]. The feedstock preparation is simple in this case: the nanopowder is added in small increments to the monomeric matrix, using a laboratory dissolver stirrer.

5.1.2 Preceramic polymer (PCP) resins

The use of photopolymerizing suspensions in vat polymerization may be difficult in some cases due to high viscosity [85]. Besides, certain ceramic powders, in particular the class of non-oxides, are colored and therefore absorb light in the UV–VIS [102] spectrum. To overcome these issues, preceramic polymers (PCPs) offer an alternative strategy. PCPs are organic compounds from which amorphous ceramic materials are obtained, precisely called polymer-derived ceramics (PDC) [103], following thermolytic decomposition. PCPs are polycarbosilanes [104], polysiloxanes [105], polysilazane [106], polysilsesquioxanes [107] and they are precursors of Si-based bicomponent (SiO_2 [108], SiC rich ceramic), Si_3N_4 [109]) and multicomponent ceramics (SiOC [104, 110, 111], SiCN [112], SiBCN [113]).

Approaches to this technique are not limited to the use of PCPs with photo-reactive acrylic functionality [110]. Photo-reactive PCPs currently available on the market are still limited; it is, therefore, common to use chemical synthesis to modify the backbone of PCP to make it photocurable, e.g., commercial silicon [107] and polyvinylsilazane [112] modified with methacrylate groups or by a sol–gel synthesis between 3-acryloxypropyl trimethoxysilane (APTMS) and tetraethyl orthosilicate (TEOS) to obtain a photocurable ink [114].

Some authors used the acrylate-vinyl (allyl) for PCP reticular and multifunctional acrylic monomers [104, 109], but also the fast curing of thiol-ene free radical addition in a system composed of polysiloxane with vinyl function and 1,6-hexanedithiol [115]. Other works propose UV curable blends of multiple PCP [111, 116], in which only one PCP participates in the crosslinking reaction, while the others contribute to increasing ceramic yield. Other variants of this

technique use filled polysiloxane feedstock. Brinckmann et al. obtained a SiOC-SiC whisker PDC in which the mere addition of 0.5 wt% filler allows to considerably limit the shrinkage and improve part stability [117]. Besides, absorbance, in the presence of the filler, may increase by order of magnitude when compared to the base resin.

5.2 Metallic feedstock

Similar to the ceramic-loaded resin, a UV curable feedstock with metal powder is prepared by incorporating metallic powder into the resin. Acrylates, epoxies, or a mixture of both can be used as a polymerizable resin. However, contrary to most ceramic powder-based feedstocks, metal powder-based feedstocks are dark in color. Therefore, in general, a high-energy source with longer exposure times is needed for polymerization. High-density metal powder is treated with dispersing agents to avoid early sedimentation of the powder and to avoid change in penetration of radiation inside the resin. The powder content is kept high to prevent cracks during the removal of organic parts in debinding. However, as discussed in the previous section, higher powder content increases the feedstock viscosity, which may not be desirable as it limits the flow of liquid resin for film formation. An increase in the viscosity is also reported as the size of the particle decreases for a given metal concentration. New DLP printers with coating/wiping blades and heating elements enable an increase in the powder content. At present, only a few studies [56, 118–120] have investigated the use of metallic suspension printed with DLP. However, a potential increase in the preparation of metal-based feedstocks can be seen to facilitate DLP technology with the competence to produce metallic parts.

6 Theoretical consideration of light-matter interaction

6.1 Light interaction of photopolymers

Light interacts with the photoinitiating system to produce reactive species. Polymerization is the result of interaction between light radiation in the UV–visible range and the photoinitiators in the resin. The radiation energy is converted into chemical energy, generating reactive agents, such as free radicals and ions. Overlapping of the absorption band of the PI and emission line of the radiation source promotes the electron in the lowest unoccupied molecular orbital (LUMO) to the highest occupied molecular orbital (HOMO). Generally, $n\pi^*$, $\pi\pi^*$, and charge transfer transitions occur in organic PI molecules [68]. In a short excited state, the photoinitiator PI^* tends to return to its original ground state by losing the energy, quenched by oxygen or monomer, or yielding to

reactive species (free radicals or ions) [65]. The formation rate of PI^* depends on the number of absorbed photons in unit time, on the fraction of PI^* , and on the fraction of PI. The number of absorbed photons is directly proportional to the light intensity. The photoinitiator absorbance is defined by Beer's law,

$$A = \epsilon lc \quad (1)$$

where ϵ is the photoinitiator molar absorptivity, l is the path length inside the PI system, and c is the PI concentration. Nonetheless, the initiation rate is not proportional to the PI concentration. From Eq. (1), when c increases, A increases proportionally. However, the amount of absorbed energy decreases exponentially along the path length, resulting in non-uniform polymerization. Hence, it is essential to find a balance between the initiation rate and the absorbance by adding the right concentration of PI, with defined molar absorptivity, to the system.

Also, the intensity of the radiation source I and the intensity inside the PI system at path length l , I_l , can be related by Beer's equation:

$$A = \ln(I/I_l) \quad (2)$$

The combination of Eqs. (1) and (2) gives:

$$l = -(1/\epsilon c) \ln(I_l/I) \quad (3)$$

Or,

$$I_l = I \exp(-l\epsilon c) \quad (4)$$

The corresponding dose of radiation D (l , t) at time t is:

$$D = tI \exp(-l\epsilon c) \quad (5)$$

The critical dose at which the polymer starts to polymerize is:

$$D_c = t_p I \exp(-l_p \epsilon c) \quad (6)$$

Thus, corresponding to the critical time:

$$T_c = D_c/I \quad (7)$$

Considering the critical radiation dose for polymerization, the thickness of the polymerized layer can be expressed as:

$$l = h \ln(t_p/T_c) \quad (8)$$

where the penetration depth h ($= 1/\epsilon c$) and critical time T_c are entirely resin, i.e., material, parameters [121], depending on the photopolymer composition, and independent of the radiation source.

6.2 Scattering in suspension-based resins

In pure photopolymers, polymerization depends on the factors defined in the previous section; however, in suspension (metal or ceramics)-based resins, the powder affects the resin interaction with the radiation. Specifically, the relevant parameters are the powder material, concentration, and size. For high-density final objects, it is necessary to have a better packing fraction, which is only possible with the high loading of small size particles. However, the high-packing fraction reduces the radiation penetration inside the system, hindering polymerization. Polymerization thickness is calculated in suspension-based resins by modifying Beer's equation [122]:

$$D_c = \frac{2\langle d \rangle n_0^2}{3Q \Delta n^2} \ln \left(\frac{E_0}{E_{crit}} \right) \quad (9)$$

where $\langle d \rangle$ is the average particle size, Q is the scattering efficiency term, and Δn is the refractive index difference between the powder and the resin. To reduce scattering and lower the polymerization time, a decrease in the powder size and a close matching between the resin and powder refractive indexes are desirable.

7 Post-processing

As briefly discussed in Sect. 2, post-processing is the last step in AM to produce a desired 3D object. One or more of the following steps may be required to: (i) clean off the residue liquid polymer from the surface, (ii) remove the support structure, (iii) polish the green body to obtain a smooth surface, and (iv) thermally treat the green body for producing dense solid object. Several finishing methods, such as vibratory finishing [123], hot cutter machining, optical polishing, micromachining process, etc., have been developed to obtain the required surface finishing [124]. Hereafter the most common post-processing phases used in DLP or SLA-based manufacturing are presented.

7.1 Cleaning of the green body

In both geometries, bottom-up and top-down, used in the DLP process, the printed object emerges from the unpolymerized resin vat, with resin residues on the printed structure. This residual resin needs to be cleaned off soon after the printing process to avoid gelation by the natural light and complete curing in further process. Generally, the green body is rinsed and sonicated in solvents like isopropyl alcohol, ethyl alcohol, or acetone. However, the high reactivity of these solvents may wear off the printed part surface in case of overexposure to the solvent. Keeping

green parts inside these solvents also generates swelling, which affects the final geometry. Tripropylene glycol monomethyl ether (TPM) and dipropylene glycol monomethyl ether (DPM) are other classes of solvents, which are less volatile and flammable compared to alcohol-based solvents [125].

7.2 Removal of the support structure

In the manufacturing of complex 3D objects from liquid or powder materials, support structures are often required [126]. Changes in the printing orientation may mitigate the necessity of support structures [127]. However, for structures such as overhangs or horizontal bridges, the use of supporting structures is almost inevitable. The slicing software enables automatic or manual generation of supports. Printed supports are removed from the green body before UV curing. Incomplete polymerization of the resin during printing makes removal steps easier. At present, multiple slicers allow different parameters for support structures and 3D objects, making the removal process easier. In general, most of the resins are fragile after the polymerization, thus it is easy to break off thin support from the bulk object.

7.3 UV curing

For polymerization of the liquid polymer layer with UV radiation, the exposure time is carefully chosen. In case the exposure is too short, photopolymer remains under cured, potentially leading to dissolution in solvents during cleaning. On the opposite, if the exposure to UV is too long, the photopolymer tends to achieve complete polymerization, leading to high adhesion between the resin and the vat base: over time, this may damage the vat base. Therefore, an ideal exposure time is needed for optimal polymerization of layers to prevent under- or complete polymerization. Indeed, post-curing of polymerized parts is done in a UV oven to ensure complete polymerization to achieve better mechanical properties [128]. However, there

is a limitation related to thicker walls of manufactured parts, across which the radiation cannot penetrate and reach the inner part. This leads to anisotropy in the degree of polymerization across the wall resulting in deformation of shape while post-curing.

7.4 Debinding

During debinding, the polymerized resin (also referred to as binder), which provides the matrix to the solid powder after polymerization, is decomposed and evaporated at high temperatures in controlled atmospheric conditions. Thermogravimetric analysis (TGA) and Fourier transform infrared (FT-IR) spectroscopy are utilized to determine the optimum heat cycle for debinding. Previous studies reported that mass loss typically starts at around 200 °C, and nearly complete organic material decomposition occurs before ~600 °C [129, 130]. Physical properties such as powder size distribution and amount of filler material also affect the debinding process. Wang et al. reported that debinding is a two-stage process: low-temperature debinding (200–300 °C) and high-temperature debinding (300–600 °C). In low-temperature debinding, the binder starts to melt, and decomposed gas flows from inside to outside via formed interconnected pores [131]. In high-temperature debinding, carbon is oxidized after binder decomposition, followed by a release of expanded CO₂, forming cracks. Slow ramps and long temperature hold may thus be required, resulting in a long debinding process (of the order of 100 h), to optimize the process and avoid cracks, especially for ceramics. In a study by Liu et al., a fast debinding process has been reported for producing silica glass [132]. Penetration tunnel formed by early-stage evaporation led material out of green part rapidly while reducing debinding time by factor three. Removal of the organic resin causes shrinkage and porosity in the debinded object. This porous, fragile 3D structure with loosely bonded solid particles needs further treatment for manufacturing dense solid objects, i.e., sintering (Fig. 9).

Fig. 9 Thermal treatment of the green body prepared with suspension-based resin. The photopolymer provides the organic matrix to the solid powder (*left*) in creating the structure. Later, this organic part is burnt in debinding process (*middle*), leaving only powder that is fused in the sintering process (*right*)

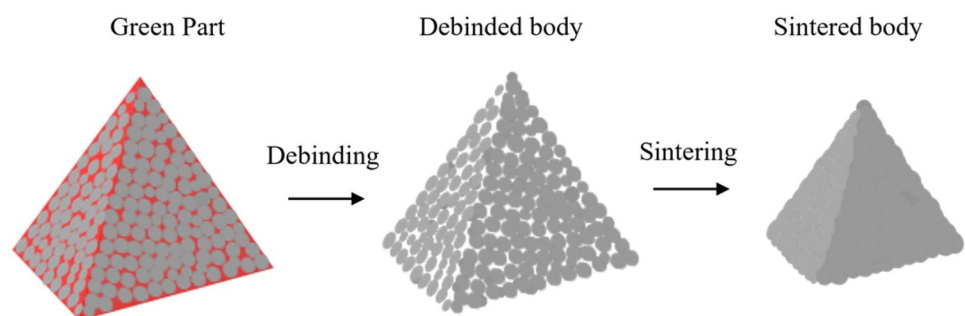


Table 3 Sintering temperature for different materials from the literature

| Powder | Particle size (μm) | Max. sintering temperature ($^{\circ}\text{C}$) | Relative density (%) | Reference |
|-------------------------------------|---------------------------------|---|----------------------|-----------|
| Zirconia (ZrO_2) | – | 1600 | 99.45 | [135] |
| Alumina (Al_2O_3) | 0.2 (d_{50}) | 1650 | 99.3 | [136] |
| Titania (TiO_2) | 1–2 | 1350 | – | [137] |
| Silica (SiO_2) | – | 1250 | – | [132] |
| Stainless Steel (SS-420) | 55/22 | 1250 | 97.5 | [56] |
| Copper (Cu) | 22 (d_{50}) | 1050 | 94 | [120] |

d_{50} is the value of the particle diameter at 50% in the cumulative distribution

7.5 Sintering

Sintering is the final stage of post-processing, where solid particles are compacted at high temperatures, producing a denser solid structure to improve mechanical properties and product quality. However, incomplete healing from the defects generated during debinding step may hinder reaching higher densities. Sintering time, temperature ramp, and hold time at constant temperature affect the intergranular bonding between particles. Low heating rates produce high relative density at a given temperature. Sintering is normally divided into three stages: (i) an early stage where no shrinkage is observed due to the merge and recrystallization of crystallites; (ii) an intermediate stage, during which particles start to adhere and grain growth is observed; (iii) a final stage, during which micropores close and densification finish [133].

Various studies on the ceramic parts sintering produced by DLP, such as zirconia ZrO_2 [134, 135], alumina Al_2O_3 [136], titania TiO_2 [137], silica SiO_2 [132] have been conducted (Table 3). Metal sintering still needs to be systematically explored in the context of the DLP process, as only a few examples are available, e.g. stainless steel [56] and copper [119, 120].

8 Applications

AM has been significantly developed from prototyping non-functional parts since it was introduced in the early 1980s. In the last decade, all manufacturing technologies have reached a significant landmark due to the development of innovative materials [23, 138] for manufacturing (Fig. 10). From micro-structures to macro fabrication, AM is taking the place of conventional manufacturing technologies in many sectors owing to the ability to generate complex, lightweight structures with high strength [139]. Aerospace, automobile, and medical sector [140] were some of the early adopters of AM because for these reasons. At present, a distinct AM technology [19] is chosen for a specific application based on the choice of the raw material. Within this framework, DLP technology is used to produce functional and non-functional parts in various application parts with unforeseen resolution in AM.

In 1995, during the early development of stereolithography-based techniques, Dickens et al. reported 100 μm of minimum layer thickness with 50 μm accuracy for rapid prototyping [148]. Kim and Hwang et al. reported a resolution of $76 \pm 14 \mu\text{m}$ in dental prototypes using a DLP printer with 70 μm of XY resolution and 75 μm

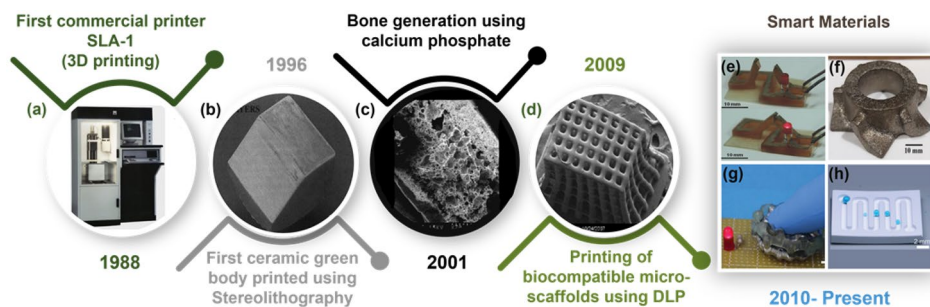


Fig. 10 Timeline of the development of materials, applications and, stereolithography technology. Block **a–d** are adapted and reprinted from Ref. [141] (with permission from Elsevier), [142] (with permission from John Wiley and Sons), [143] (with permission from John Wiley and Sons) and [144] (with permission from Elsevier),

respectively. Block **e–h** are adapted and reprinted from [145] (with permission from John Wiley and Sons), [56] (with permission from Elsevier), [146] (with permission from John Wiley and Sons) and [147] (licensed under a Creative Commons license, CC BY-NC 4.0), respectively

layer thickness [149]. Among projection-based technologies, Januszewicz et al. introduced the CLIP method of AM using 0.4 μm slice thickness. The advancements in dimensional accuracy with high precision of manufactured objects made DLP the best choice to create prototypes and casts [57].

Biocompatibility of ceramic powders, such as zirconia [134] and alumina [150], opened the way to the use of DLP-printed ceramics for medical applications. The technology is popular among dentists to customize orthodontic models and develop implants, bridges, and teeth [151]. Apart from dentistry, ceramic-based DLP manufacturing technology is also used for producing bone scaffolds for bone regeneration. Christina et al. used tricalcium phosphate ceramic powder to produce bone scaffolds using DLP [152]. In another work by Liu et al., hydroxyapatite (HA) bioceramic was used for manufacturing bone scaffolds [153]. In recent works, the manufacturing of transparent glass has been reported by low-cost DLP technology using ceramic-based resin [114, 154]. In a work by Rodríguez et al., fuel cell components have been manufactured using yttria-stabilized zirconia-based feedstock [155]. High melting point, working temperature, and lightweight with excellent mechanical properties allow ceramic parts for myriad applications [111, 156, 157].

Another application of the low power source DLP technology is bioprinting of living tissues [69] using functional biopolymers and synthetic polymers [158]. In a recent study by Kim et al., UV curable silk fibroin bioink has been developed to generate organ structures [159]. Lu et al. used an acrylate-based photocurable resin as a scaffold, and murine bone marrow-derived cells incorporated on fibronectin functionalized scaffolds using DLP [160]. Review articles by Zhu et al. and Vincula et al. demonstrated extended applications and progress in tissue engineering using AM technologies [161, 162].

With the advancement in materials for DLP, researchers also introduced smart printable materials, such as elastomers. Elastomers have good mechanical properties and can provide thermal and electrical insulation and, in some cases, self-healing capabilities, which is interesting for electronics, wearables, soft robotics, etc. Traugutt et al. used the DLP technology for manufacturing complex liquid crystal elastomer (LCE) structures for strain energy dissipation [163]. In another work by Patel et al., DLP printed the so-called stretchable and UV printed (SUV) elastomer, with a reported 1100% strain. The printed object can be used for soft and deformable structures [146]. Zhao et al. reported manufacturing of silicone elastomers with 1400% strain. The geometry is then applied with carbon nanotubes-doped hydrogel for possible application in stretchable electronics [164].

DLP has also been exploited with composite-based photopolymers. Photopolymers reinforced with glass fibers, graphene nanoparticles, silicon carbide, zinc oxide, and

multi-walled carbon nanotubes are used for manufacturing 3D objects with different functionalities [77]. Mu et al. introduced multi-walled carbon nanotube (MWCNT)-based polymeric composites to produce electrically conductive objects, which can be used as capacitive sensors, stretchable circuits, and shape memory devices [43]. Yunus et al. presented DLP-printed nanocomposite reinforced samples using copper, magnetite nanoparticles, and carbon nanofiber via aligning and condensing conductive nanoparticles for producing embedded electronic components [165].

Wu et al. presented the printing of a novel acrylate-based shape memory polymer via DLP [166]. Zhou et al. printed a piezoelectric nanogenerator for self-power sensor application using barium titanate polymer-based composite [167]. Zhu et al. mentioned DLP printing of healable and recyclable polymers for various applications [168]. High-resolution printing DLP technology also enables the manufacturing of microfluidic devices [169, 170]. For sensing applications, DLP has been exploited for the fabrication of optical devices such as optical fibers [171] and lenses [172]. Recently, the technology has been used to fabricate superhydrophobic objects with pillar structures [147, 173].

9 Conclusions and future perspectives

In this review, we focused on the characteristics and potential of DLP within the wide landscape of additive manufacturing technologies. DLP combines high manufacturing speed with precision, using a variety of materials, ranging from pure resins to ceramic- and metal-loaded suspensions. The review elucidates the detailed working principles of the DLP manufacturing process, describing the fundamentals of material interaction with the light source.

The potential of manufacturing complex functional and non-functional parts using polymers, suspensions, and functional materials attracted the interest of several industrial fields, including dentistry, tissue engineering, electronics, and microfluidics. Also, 4D printing, enabling the fabrication of new materials that change their properties under external stimuli, is a growing field that demonstrates a huge potential in the manufacturing of sensors and actuators, e.g. for robotics and smart wearables [174]. Optimized printing systems, innovative methods, and newly engineered materials left behind major printing limitations, time, complexity, and materials.

However, there are still some challenges in adopting DLP, as well as other AM technologies, and substituting conventional technologies [175–177]. Among them, one of the questions is the scale of production, which is still limited: from a few microns to a few millimeters. Micro projection stereolithography seems promising in the fabrication of micro features [178] while optimizing printing quality:

however, a trade-off exists between size and precision, due to the limited projected area of the DLP source. Another challenge for DLP is the time-consuming separation (and recoating for viscous suspensions) step of the cured layer. Few methods, such as CLIP [57], HARP [58], and tunable pre-curing DLP [179], have evolved to eliminate this time-consuming step but for highly concentrated suspensions (ceramics, metals, and composites) the problem still needs to be addressed. Multi-material printing is still a question for this technology along with other AM methods. To date, there is no commercial system available for multi-materials printing with critical cleaning steps during material swapping to avoid cross-contamination. For suspension-based manufacturing of solid parts, the thermal treatment, debinding, and sintering, have still been a challenge in producing dense solid structures with this technology. The fact that very little research in metallic suspension-based manufacturing has been reported so far not only calls for more efforts in DLP-based metal printing but also opens other research opportunities for metallurgy. All these challenges need to be carefully addressed and will promote further research and development on DLP technology in the next coming years.

Acknowledgements RC and CA acknowledge PhD funding from Regione Lombardia under the program “Laboratorio sui Materiali e processi industriali sostenibili 4.0” (Accordo di collaborazione RL-ENEA). CA acknowledges partial support from the Italian Ministry for University and Research (MIUR) through the Rita Levi Montalcini fellowship for young researchers.

Funding Open access funding provided by Università degli Studi di Milano - Bicocca within the CRUI-CARE Agreement.

Open Access This article is licensed under a Creative Commons Attribution 4.0 International License, which permits use, sharing, adaptation, distribution and reproduction in any medium or format, as long as you give appropriate credit to the original author(s) and the source, provide a link to the Creative Commons licence, and indicate if changes were made. The images or other third party material in this article are included in the article's Creative Commons licence, unless indicated otherwise in a credit line to the material. If material is not included in the article's Creative Commons licence and your intended use is not permitted by statutory regulation or exceeds the permitted use, you will need to obtain permission directly from the copyright holder. To view a copy of this licence, visit <http://creativecommons.org/licenses/by/4.0/>.

References

- Gebhardt A, Hötter J-S (2016) Basics, definitions, and application levels. Additive manufacturing. Carl Hanser Verlag GmbH & Co. KG, München, pp 1–19
- Hull CW, Arcadia (1986) Apparatus for production of three-dimensional objects by stereolithography
- Dilberoglu UM, Gharehpapagh B, Yaman U, Dolen M (2017) The role of additive manufacturing in the era of industry 4.0. *Procedia Manuf* 11:545–554. <https://doi.org/10.1016/j.promfg.2017.07.148>
- Lasi H, Fettke P, Kemper HG et al (2014) Industry 4.0. *Bus Inf Syst Eng* 6:239–242. <https://doi.org/10.1007/s12599-014-0334-4>
- Duda T, Raghavan LV (2016) 3D metal printing technology. *IFAC-PapersOnLine* 49:103–110. <https://doi.org/10.1016/j.ifacol.2016.11.111>
- Ford S, Despeisse M (2016) Additive manufacturing and sustainability: an exploratory study of the advantages and challenges. *J Clean Prod*. <https://doi.org/10.1016/j.jclepro.2016.04.150>
- Chadha U, Abrol A, Vora NP et al (2022) Performance evaluation of 3D printing technologies: a review, recent advances, current challenges, and future directions. *Prog Addit Manuf*. <https://doi.org/10.1007/s40964-021-00257-4>
- Bhargav A, Sanjairaj V, Rosa V et al (2018) Applications of additive manufacturing in dentistry: a review. *J Biomed Mater Res - Part B Appl Biomater* 106:2058–2064. <https://doi.org/10.1002/jbm.b.33961>
- Singh S, Ramakrishna S (2017) Biomedical applications of additive manufacturing: present and future. *Curr Opin Biomed Eng* 2:105–115
- da Silva LRR, Sales WF, Campos FDAR et al (2021) A comprehensive review on additive manufacturing of medical devices. *Prog Addit Manuf* 6:517–553. <https://doi.org/10.1007/s40964-021-00188-0>
- Srivastava M, Rathee S, Maheshwari S, Kundra TK (2019) Additive manufacturing applications. Additive manufacturing. CRC Press, Florida, pp 235–258
- Carpenter C (2015) Additive manufacturing for the space industry. Additive manufacturing. CRC Press, Boca Raton, FL, pp 290–309
- Buchanan C, Gardner L (2019) Metal 3D printing in construction: a review of methods, research, applications, opportunities and challenges. *Eng Struct* 180:332–348
- Bourell D, Kruth JP, Leu M et al (2017) Materials for additive manufacturing. *CIRP Ann* 66:659–681. <https://doi.org/10.1016/j.cirp.2017.05.009>
- Pei E, Loh GH, Harrison D et al (2017) A study of 4D printing and functionally graded additive manufacturing. *Assem Autom* 37:147–153. <https://doi.org/10.1108/AA-01-2017-012>
- Rathee S, Srivastava M, Maheshwari S et al (2018) Friction based additive manufacturing technologies. CRC Press/Taylor & Francis Group, Boca Raton, FL
- Srivastava M, Rathee S, Maheshwari S et al (2019) A review on recent progress in solid state friction based metal additive manufacturing: friction stir additive techniques. *Crit Rev Solid State Mater Sci* 44:345–377
- Ligon SC, Liska R, Stampfl J et al (2017) Polymers for 3D printing and customized additive manufacturing. *Chem Rev* 117:10212–10290. <https://doi.org/10.1021/acs.chemrev.7b00074>
- Redwood B, Schöffner F, Garret B (2017) The 3D printing handbook: technologies, design and applications. 3D Hubs, Amsterdam
- Gebhardt A, Hötter J-S (2016) Additive manufacturing. In: Additive manufacturing. Carl Hanser Verlag GmbH & Co. KG, München, pp I–XX
- Calignano F, Manfredi D, Ambrosio EP et al (2017) Overview on additive manufacturing technologies. *Proc IEEE* 105:593–612. <https://doi.org/10.1109/JPROC.2016.2625098>
- Wong KV, Hernandez A (2012) A review of additive manufacturing. *ISRN Mech Eng* 2012:1–10. <https://doi.org/10.5402/2012/208760>
- Lee JY, An J, Chua CK (2017) Fundamentals and applications of 3D printing for novel materials. *Appl Mater Today* 7:120–133. <https://doi.org/10.1016/j.apmt.2017.02.004>

24. Sing SL, Yeong WY, Wiria FE et al (2017) Direct selective laser sintering and melting of ceramics: a review. *Rapid Prototyp J* 23:611–623. <https://doi.org/10.1108/RPJ-11-2015-0178>
25. Kruth JP, Wang X, Laoui T, Froyen L (2003) Lasers and materials in selective laser sintering. *Assem Autom* 23:357–371. <https://doi.org/10.1108/01445150310698652>
26. Yap CY, Chua CK, Dong ZL et al (2015) Review of selective laser melting: materials and applications. *Appl Phys Rev* 2:41101
27. Rafi HK, Starr TL, Stucker BE (2013) A comparison of the tensile, fatigue, and fracture behavior of Ti–6Al–4V and 15–5 PH stainless steel parts made by selective laser melting. *Int J Adv Manuf Technol* 69:1299–1309. <https://doi.org/10.1007/s00170-013-5106-7>
28. Murr LE, Gaytan SM, Ramirez DA et al (2012) Metal fabrication by additive manufacturing using laser and electron beam melting technologies. *J Mater Sci Technol* 28:1–14
29. Körner C (2016) Additive manufacturing of metallic components by selective electron beam melting - a review. *Int Mater Rev* 61:361–377
30. Izadi M, Farzaneh A, Mohammed M et al (2020) A review of laser engineered net shaping (LENS) build and process parameters of metallic parts. *Rapid Prototyp J* 26:1059–1078. <https://doi.org/10.1108/RPJ-04-2018-0088/FULL/PDF>
31. Li Y, Hu Y, Cong W et al (2017) Additive manufacturing of alumina using laser engineered net shaping: effects of deposition variables. *Ceram Int* 43:7768–7775. <https://doi.org/10.1016/j.ceramint.2017.03.085>
32. Ziaee M, Crane NB (2019) Binder jetting: a review of process, materials, and methods. *Addit Manuf* 28:781–801. <https://doi.org/10.1016/j.addma.2019.05.031>
33. Lv X, Ye F, Cheng L et al (2019) Binder jetting of ceramics: powders, binders, printing parameters, equipment, and post-treatment. *Ceram Int* 45:12609–12624
34. Ahn D, Kweon JH, Choi J, Lee S (2012) Quantification of surface roughness of parts processed by laminated object manufacturing. *J Mater Process Technol* 212:339–346. <https://doi.org/10.1016/j.jmatprotec.2011.08.013>
35. Dermeik B, Travitzky N (2020) Laminated object manufacturing of ceramic-based materials. *Adv Eng Mater* 22:2000256
36. Mohamed OA, Masood SH, Bhowmik JL (2015) Optimization of fused deposition modeling process parameters: a review of current research and future prospects. *Adv Manuf* 3:42–53. <https://doi.org/10.1007/s40436-014-0097-7>
37. Daminabo SC, Goel S, Grammatikos SA et al (2020) Fused deposition modeling-based additive manufacturing (3D printing): techniques for polymer material systems. *Mater Today Chem* 16:100248. <https://doi.org/10.1016/j.mtchem.2020.100248>
38. Srivastava M, Rathee S (2018) Optimisation of FDM process parameters by Taguchi method for imparting customised properties to components. *Virtual Phys Prototyp* 13:203–210. <https://doi.org/10.1080/17452759.2018.1440722>
39. Castiaux AD, Pinger CW, Hayter EA et al (2019) PolyJet 3D-printed enclosed microfluidic channels without photocurable supports. *Anal Chem* 91:6910–6917. https://doi.org/10.1021/ACS.ANALCHEM.9B01302/SUPPL_FILE/AC9B01302_SI_002.ZIP
40. Cazón A, Morer P, Matey L (2014) PolyJet technology for product prototyping: tensile strength and surface roughness properties. *Proc Inst Mech Eng Part B J Eng Manuf* 228:1664–1675. <https://doi.org/10.1177/0954405413518515>
41. Bártolo PJ (2011) Stereolithographic processes. *Stereolithography*. Springer, Boston, MA, pp 1–36
42. Pagac M, Hajnys J, Ma Q-P et al (2021) A review of vat photopolymerization technology: materials, applications, challenges, and future trends of 3D printing. *Polymers (Basel)* 13:598. <https://doi.org/10.3390/polym13040598>
43. Mu Q, Wang L, Dunn CK et al (2017) Digital light processing 3D printing of conductive complex structures. *Addit Manuf* 18:74–83. <https://doi.org/10.1016/j.addma.2017.08.011>
44. Kuang X, Wu J, Chen K et al (2019) Grayscale digital light processing 3D printing for highly functionally graded materials. *Sci Adv* 5:eaav5790. <https://doi.org/10.1126/sciadv.aav5790>
45. Hornbeck LJ (1999) Digital light processing update: status and future applications. In: Wu MH (ed) *Projection displays V*. pp 158–170
46. Monk DW, Gale RO (1995) The digital micromirror device for projection display. *Microelectron Eng* 27:489–493. [https://doi.org/10.1016/0167-9317\(94\)00151-J](https://doi.org/10.1016/0167-9317(94)00151-J)
47. Santoliquido O, Colombo P, Ortona A (2019) Additive manufacturing of ceramic components by digital light processing: a comparison between the “bottom-up” and the “top-down” approaches. *J Eur Ceram Soc* 39:2140–2148. <https://doi.org/10.1016/j.jeurceramsoc.2019.01.044>
48. Wu X, Xu C, Zhang Z (2021) Flexible film separation analysis of LCD based mask stereolithography. *J Mater Process Technol* 288:116916. <https://doi.org/10.1016/j.jmatprotec.2020.116916>
49. Wu L, Dong Z, Du H et al (2018) Bioinspired ultra-low adhesive energy interface for continuous 3D printing: reducing curing induced adhesion. *Research* 2018:1–10. <https://doi.org/10.1155/2018/4795604>
50. Walker DA, Hedrick JL, Mirkin CA (2019) Rapid, large-volume, thermally controlled 3D printing using a mobile liquid interface. *Science* 366:360–364. <https://doi.org/10.1126/science.aax1562>
51. Xu Y, Zhu Y, Sun Y et al (2021) A vibration-assisted separation method for constrained-surface-based stereolithography. *J Manuf Sci Eng*. <https://doi.org/10.1115/1.4048445>
52. Wu X, Lian Q, Li D, Jin Z (2017) Tilting separation analysis of bottom-up mask projection stereolithography based on cohesive zone model. *J Mater Process Technol* 243:184–196. <https://doi.org/10.1016/j.jmatprotec.2016.12.016>
53. Wicker RB, MacDonald EW (2012) Multi-material, multi-technology stereolithography. *Virtual Phys Prototyp* 7:181–194. <https://doi.org/10.1080/17452759.2012.721119>
54. Ge Q, Sakhaei AH, Lee H et al (2016) Multimaterial 4D printing with tailorable shape memory polymers. *Sci Rep* 6:31110. <https://doi.org/10.1038/srep31110>
55. Peng X, Kuang X, Roach DJ et al (2021) Integrating digital light processing with direct ink writing for hybrid 3D printing of functional structures and devices. *Addit Manuf* 40:101911. <https://doi.org/10.1016/j.addma.2021.101911>
56. Nguyen HX, Suen H, Poudel B et al (2020) Development of an innovative, high speed, large-scaled, and affordable metal additive manufacturing process. *CIRP Ann* 69:177–180. <https://doi.org/10.1016/j.cirp.2020.04.069>
57. Januszewicz R, Tumbleston JR, Quintanilla AL et al (2016) Layerless fabrication with continuous liquid interface production. *Proc Natl Acad Sci U S A* 113:11703–11708. <https://doi.org/10.1073/pnas.1605271113>
58. Walker DA, Hedrick JL, Mirkin CA (2019) Rapid, large-volume, thermally controlled 3D printing using a mobile liquid interface. *Science* (80-) 366:360–364. <https://doi.org/10.1126/science.aax1562>
59. Kelly BE, Bhattacharya I, Heidari H et al (2019) Volumetric additive manufacturing via tomographic reconstruction. *Science* 363:1075–1079. <https://doi.org/10.1126/science.aau7114>
60. Raimondi MT, Eaton SM, Nava MM et al (2012) Two-photon laser polymerization: from fundamentals to biomedical application in tissue engineering and regenerative medicine. *J Appl Biomater Funct Mater* 10:55–65. <https://doi.org/10.5301/JABFM.2012.9278>

61. Bunea A-I, del Castillo IN, Droumpali A et al (2021) Micro 3D printing by two-photon polymerization: configurations and parameters for the nanoscribe system. *Micro* 1:164–180. <https://doi.org/10.3390/micro1020013>
62. Choi JW, Kim HC, Wicker R (2011) Multi-material stereolithography. *J Mater Process Technol* 211:318–328. <https://doi.org/10.1016/J.JMATPROTEC.2010.10.003>
63. Liska R, Schuster M, Inführ R et al (2007) Photopolymers for rapid prototyping. *J Coat Technol Res* 4:505–510. <https://doi.org/10.1007/s11998-007-9059-3>
64. Arsu N, Aydin M, Yagci Y, et al (2006) One component thioxanthone based Type II photoinitiators. In: *Photochemistry and UV curing: new trends*, pp 1–13
65. Bean AJ (1992) *Radiation curing of printing inks*. Radiation curing. Springer, Boston, MA, pp 301–332
66. Decker C (1996) Photoinitiated crosslinking polymerisation. *Prog Polym Sci* 21:593–650
67. Fouassier JP, Morlet-Savary F, Lalevée J et al (2010) Dyes as photoinitiators or photosensitizers of polymerization reactions. *Materials (Basel)* 3:5130–5142
68. Fouassier JP, Lalevée J (2012) *Photoinitiators for polymer synthesis: scope reactivity and efficiency*. Wiley-VCH Verlag GmbH & Co KGaA, Weinheim
69. Shafiee A, Atala A (2017) Tissue engineering: toward a new era of medicine. *Annu Rev Med* 68:29–40. <https://doi.org/10.1146/annurev-med-102715-092331>
70. Pan X, Tasdelen MA, Laun J et al (2016) Photomediated controlled radical polymerization. *Prog Polym Sci* 62:73–125
71. Szwarc M, Van Beylen M (1993) *Ionic polymerization and living polymers*. Springer, Dordrecht
72. Mendes-Felipe C, Oliveira J, Etxebarria I et al (2019) State-of-the-art and future challenges of UV curable polymer-based smart materials for printing technologies. *Adv Mater Technol* 4:1800618
73. Crivello JV (1999) The discovery and development of onium salt cationic photoinitiators. *J Polym Sci Part A Polym Chem* 37:4241–4254. [https://doi.org/10.1002/\(SICI\)1099-0518\(19991201\)37:23%3c4241::AID-POLA1%3e3.0.CO;2-R](https://doi.org/10.1002/(SICI)1099-0518(19991201)37:23%3c4241::AID-POLA1%3e3.0.CO;2-R)
74. Schnabel W (2007) *Polymers and light*. Wiley, Weinheim
75. Bagheri A, Jin J (2019) Photopolymerization in 3D printing. *ACS Appl Polym Mater* 1:593–611
76. Yagci Y, Jockusch S, Turro NJ (2010) Photoinitiated polymerization: advances, challenges, and opportunities. *Macromolecules* 43:6245–6260
77. Clarissa WHY, Chia CH, Zakaria S, Evyan YCY (2021) Recent advancement in 3-D printing: nanocomposites with added functionality. *Prog Addit Manuf* 2021:1–26. <https://doi.org/10.1007/S40964-021-00232-Z>
78. Nam S, Pei E (2019) A taxonomy of shape-changing behavior for 4D printed parts using shape-memory polymers. *Prog Addit Manuf* 4:167–184. <https://doi.org/10.1007/S40964-019-00079-5/FIGURES/28>
79. Halloran JW (2016) Ceramic stereolithography: additive manufacturing for ceramics by photopolymerization. *Annu Rev Mater Res* 46:19–40. <https://doi.org/10.1146/annurev-matsci-070115-031841>
80. Ventura SC, Narang SC, Sharma S, Stotts J (1996) A new sff process for functional ceramic components. In: *Solid freeform fabrication symp. Proc.*, pp 327–334
81. Hinczewski C, Corbel S, Chartier T (1998) Ceramic suspensions suitable for stereolithography. *J Eur Ceram Soc* 18:583–590. [https://doi.org/10.1016/s0955-2219\(97\)00186-6](https://doi.org/10.1016/s0955-2219(97)00186-6)
82. Griffith ML, Halloran JW (2005) Freeform fabrication of ceramics via stereolithography. *J Am Ceram Soc* 79:2601–2608. <https://doi.org/10.1111/j.1151-2916.1996.tb09022.x>
83. Badev A, Abouliatim Y, Chartier T et al (2011) Photopolymerization kinetics of a polyether acrylate in the presence of ceramic fillers used in stereolithography. *J Photochem Photobiol A Chem* 222:117–122. <https://doi.org/10.1016/j.jphotochem.2011.05.010>
84. Halloran JW, Tomeckova V, Gentry S et al (2011) Photopolymerization of powder suspensions for shaping ceramics. *J Eur Ceram Soc* 31:2613–2619. <https://doi.org/10.1016/j.jeurceramsoc.2010.12.003>
85. Jang JH, Wang S, Pilgrim SM, Schulze WA (2000) Preparation and characterization of barium titanate suspensions for stereolithography. *J Am Ceram Soc* 83:1804–1806. <https://doi.org/10.1111/j.1151-2916.2000.tb01467.x>
86. Tomeckova V, Halloran JW (2011) Flow behavior of polymerizable ceramic suspensions as function of ceramic volume fraction and temperature. *J Eur Ceram Soc* 31:2535–2542. <https://doi.org/10.1016/j.jeurceramsoc.2011.01.019>
87. Gmeiner R, Mitterramskogler G, Stampfl J, Boccaccini AR (2015) Stereolithographic ceramic manufacturing of high strength bioactive glass. *Int J Appl Ceram Technol* 12:38–45. <https://doi.org/10.1111/ijac.12325>
88. Komissarenko D, Sokolov P, Evstigneeva A et al (2018) Rheological and curing behavior of acrylate-based suspensions for the DLP 3D printing of complex zirconia parts. *Materials (Basel)* 11:2350. <https://doi.org/10.3390/ma11122350>
89. Tomeckova V, Teyssandier F, Norton SJ et al (2012) Photopolymerization of acrylate suspensions. *J Photochem Photobiol A Chem* 247:74–81. <https://doi.org/10.1016/j.jphotochem.2012.08.008>
90. Chartier T, Badev A, Abouliatim Y et al (2012) Stereolithography process: Influence of the rheology of silica suspensions and of the medium on polymerization kinetics - cured depth and width. *J Eur Ceram Soc* 32:1625–1634. <https://doi.org/10.1016/j.jeurceramsoc.2012.01.010>
91. Zhang K, He R, Ding G et al (2020) Digital light processing of 3Y-TZP strengthened ZrO₂ ceramics. *Mater Sci Eng A* 774:138768. <https://doi.org/10.1016/j.msea.2019.138768>
92. Liu W, Wu H, Tian Z et al (2019) 3D printing of dense structural ceramic microcomponents with low cost: tailoring the sintering kinetics and the microstructure evolution. *J Am Ceram Soc* 102:2257–2262. <https://doi.org/10.1111/jace.16241>
93. An D, Li H, Xie Z et al (2017) Additive manufacturing and characterization of complex Al₂O₃ parts based on a novel stereolithography method. *Int J Appl Ceram Technol* 14:836–844. <https://doi.org/10.1111/ijac.12721>
94. Zhang S, Sha N, Zhao Z (2017) Surface modification of α -Al₂O₃ with dicarboxylic acids for the preparation of UV-curable ceramic suspensions. *J Eur Ceram Soc* 37:1607–1616. <https://doi.org/10.1016/j.jeurceramsoc.2016.12.013>
95. Wang Y, Wang Z, Liu S et al (2019) Additive manufacturing of silica ceramics from aqueous acrylamide based suspension. *Ceram Int* 45:21328–21332. <https://doi.org/10.1016/j.ceramint.2019.07.118>
96. Borlaf M, Szubra N, Serra-capdevila A et al (2020) Fabrication of ZrO₂ and ATZ materials via UV-LCM-DLP additive manufacturing technology. *J Eur Ceram Soc* 40:1574–1581. <https://doi.org/10.1016/j.jeurceramsoc.2019.11.037>
97. Li X, Zhong H, Zhang J et al (2020) Fabrication of zirconia all-ceramic crown via DLP-based stereolithography. *Int J Appl Ceram Technol* 17:844–853. <https://doi.org/10.1111/ijac.13441>
98. Li K, Zhao Z (2017) The effect of the surfactants on the formulation of UV-curable SLA alumina suspension. *Ceram Int* 43:4761–4767. <https://doi.org/10.1016/j.ceramint.2016.11.143>
99. De Hazan Y, Heinecke J, Weber A, Graule T (2009) High solids loading ceramic colloidal dispersions in UV curable media via

- comb-polyelectrolyte surfactants. *J Colloid Interface Sci* 337:66–74. <https://doi.org/10.1016/j.jcis.2009.05.012>
100. Kotz F, Arnold K, Bauer W et al (2017) Three-dimensional printing of transparent fused silica glass. *Nature* 544:337–339. <https://doi.org/10.1038/nature22061>
 101. Cai P, Guo L, Wang H et al (2020) Effects of slurry mixing methods and solid loading on 3D printed silica glass parts based on DLP stereolithography. *Ceram Int* 46:16833–16841. <https://doi.org/10.1016/j.ceramint.2020.03.260>
 102. Ding G, He R, Zhang K et al (2019) Stereolithography-based additive manufacturing of gray-colored SiC ceramic green body. *J Am Ceram Soc* 102:7198–7209. <https://doi.org/10.1111/jace.16648>
 103. Riedel R, Mera G, Hauser R, Klonczynski A (2006) Silicon-based polymer-derived ceramics: synthesis properties and applications—a review. *J Ceram Soc Japan* 114:425–444
 104. de Hazan Y, Penner D, De HY, Penner D (2017) SiC and SiOC ceramic articles produced by stereolithography of acrylate modified polycarbosilane systems. *J Eur Ceram Soc* 37:5205–5212. <https://doi.org/10.1016/j.jeurceramsoc.2017.03.021>
 105. Li Z, Chen Z, Liu J et al (2020) Additive manufacturing of lightweight and high-strength polymer-derived SiOC ceramics. *Virtual Phys Prototyp* 15:163–177. <https://doi.org/10.1080/17452759.2019.1710919>
 106. Gao Y, Mera G, Nguyen H et al (2012) Processing route dramatically influencing the nanostructure of carbon-rich SiCN and SiBCN polymer-derived ceramics. Part I: low temperature thermal transformation. *J Eur Ceram Soc* 32:1857–1866. <https://doi.org/10.1016/j.jeurceramsoc.2011.09.012>
 107. Zanchetta E, Cattaldo M, Franchin G et al (2016) Stereolithography of SiOC ceramic microcomponents. *Adv Mater* 28:370–376. <https://doi.org/10.1002/adma.201503470>
 108. Schmidt J, Alpay A, Schwentenwein M, Colombo P (2019) Complex mullite structures fabricated via digital light processing of a preceramic polysiloxane with active alumina fillers. *J Eur Ceram Soc* 39:1336–1343. <https://doi.org/10.1016/j.jeurceramsoc.2018.11.038>
 109. Wang M, Xie C, He R et al (2019) Polymer-derived silicon nitride ceramics by digital light processing based additive manufacturing. *J Am Ceram Soc* 102:5117–5126. <https://doi.org/10.1111/jace.16389>
 110. Brigo L, Schmidt JEM, Gandin A et al (2018) 3D nanofabrication of SiOC ceramic structures. *Adv Sci* 5:1800937. <https://doi.org/10.1002/advs.201800937>
 111. Schmidt J, Colombo P (2018) Digital light processing of ceramic components from polysiloxanes. *J Eur Ceram Soc* 38:57–66. <https://doi.org/10.1016/j.jeurceramsoc.2017.07.033>
 112. Pham TA, Kim DP, Lim TW et al (2006) Three-dimensional SiCN ceramic microstructures via nano-stereolithography of inorganic polymer photoresists. *Adv Funct Mater* 16:1235–1241. <https://doi.org/10.1002/adfm.200600009>
 113. Li S, Duan W, Zhao T et al (2018) The fabrication of SiBCN ceramic components from preceramic polymers by digital light processing (DLP) 3D printing technology. *J Eur Ceram Soc* 38:4597–4603. <https://doi.org/10.1016/j.jeurceramsoc.2018.06.046>
 114. Cooperstein I, Shukrun E, Press O et al (2018) Additive manufacturing of transparent silica glass from solutions. *ACS Appl Mater Interfaces* 10:18879–18885. <https://doi.org/10.1021/acsami.8b03766>
 115. Wang X, Schmidt F, Hanaor D et al (2019) Additive manufacturing of ceramics from preceramic polymers: a versatile stereolithographic approach assisted by thiol-ene click chemistry. *Addit Manuf* 27:80–90. <https://doi.org/10.1016/j.addma.2019.02.012>
 116. Eckel ZC, Zhou C, Martin JH et al (2016) Additive manufacturing of polymer-derived ceramics. *Science* (80-) 351:58–62. <https://doi.org/10.1126/science.aad2688>
 117. Brinckmann SA, Patra N, Yao J et al (2018) Stereolithography of SiOC polymer-derived ceramics filled with SiC micronwhiskers. *Adv Eng Mater* 20:1–10. <https://doi.org/10.1002/adem.20180593>
 118. Bartolo PJ, Gaspar J (2008) Metal filled resin for stereolithography metal part. *CIRP Ann* 57:235–238. <https://doi.org/10.1016/j.cirp.2008.03.124>
 119. Lee JW, Lee IH, Cho DW (2006) Development of micro-stereolithography technology using metal powder. *Microelectron Eng* 83:1253–1256. <https://doi.org/10.1016/J.MEE.2006.01.192>
 120. Roumanie M, Flassayer C, Resch A et al (2021) Influence of debinding and sintering conditions on the composition and thermal conductivity of copper parts printed from highly loaded photocurable formulations. *SN Appl Sci* 3:1–11. <https://doi.org/10.1007/S42452-020-04049-3/FIGURES/12>
 121. Jacobs P (1992) Rapid prototyping & manufacturing—fundamentals of stereolithography. Society of Manufacturing Engineers, Dearborn
 122. Griffith ML, Halloran JW (1997) Scattering of ultraviolet radiation in turbid suspensions. *J Appl Phys* 81:2538–2546. <https://doi.org/10.1063/1.364311>
 123. Spencer JD, Cobb RC, Dickens PM (1993) Vibratory finishing of stereolithography parts. In: *Int Solid Free Fabr Symp.* <https://doi.org/10.15781/T2DJ5906T>
 124. Kumbhar NN, Mulay AV (2018) Post processing methods used to improve surface finish of products which are manufactured by additive manufacturing technologies: a review. *J Inst Eng Ser C* 99:481–487. <https://doi.org/10.1007/s40032-016-0340-z>
 125. Mostafavi D, Methani MM, Piedra-Cascón W et al (2021) Influence of the rinsing postprocessing procedures on the manufacturing accuracy of vat-polymerized dental model material. *J Prosthodont* 30:610–616. <https://doi.org/10.1111/JOPR.13288>
 126. Piedra-Cascón W, Krishnamurthy VR, Att W, Revilla-León M (2021) 3D printing parameters, supporting structures, slicing, and post-processing procedures of vat-polymerization additive manufacturing technologies: a narrative review. *J Dent* 109:103630. <https://doi.org/10.1016/J.JDENT.2021.103630>
 127. Unkovskiy A, Bui PHB, Schille C et al (2018) Objects build orientation, positioning, and curing influence dimensional accuracy and flexural properties of stereolithographically printed resin. *Dent Mater* 34:e324–e333. <https://doi.org/10.1016/J.DENTAL.2018.09.011>
 128. Riccio C, Civera M, Ruiz OG et al (2021) Effects of curing on photosensitive resins in SLA additive manufacturing. *Appl Mech* 2:942–955. <https://doi.org/10.3390/APPLMECH2040055>
 129. Wang JC, Dommati H (2018) Fabrication of zirconia ceramic parts by using solvent-based slurry stereolithography and sintering. *Int J Adv Manuf Technol* 98(5):1537–1546. <https://doi.org/10.1007/S00170-018-2349-3>
 130. Cai P, Guo L, Wang H et al (2020) Effects of slurry mixing methods and solid loading on 3D printed silica glass parts based on DLP stereolithography. *Ceram Int*. <https://doi.org/10.1016/j.ceramint.2020.03.260>
 131. Wang K, Qiu M, Jiao C et al (2020) Study on defect-free debinding green body of ceramic formed by DLP technology. *Ceram Int* 46:2438–2446. <https://doi.org/10.1016/J.CERAMINT.2019.09.237>
 132. Liu C, Qian B, Liu X et al (2018) Additive manufacturing of silica glass using laser stereolithography with a top-down approach and fast debinding. *RSC Adv* 8:16344–16348. <https://doi.org/10.1039/C8RA02428F>
 133. Kuang X, Carotenuto G, Nicolais L (1997) Review of ceramic sintering and suggestions on reducing sintering temperatures.

- Adv Perform Mater 4:257–274. <https://doi.org/10.1023/A:1008621020555>
134. He R, Liu W, Wu Z et al (2018) Fabrication of complex-shaped zirconia ceramic parts via a DLP- stereolithography-based 3D printing method. *Ceram Int* 44:3412–3416. <https://doi.org/10.1016/j.ceramint.2017.11.135>
 135. Wang J-C, Dommati H (2018) Fabrication of zirconia ceramic parts by using solvent-based slurry stereolithography and sintering. *Int J Adv Manuf Technol* 98:1537–1546. <https://doi.org/10.1007/s00170-018-2349-3>
 136. Schwentenwein M, Homa J (2015) Additive manufacturing of dense alumina ceramics. *Int J Appl Ceram Technol* 12:1–7. <https://doi.org/10.1111/IJAC.12319>
 137. Guo J, Zeng Y, Li P, Chen J (2019) Fine lattice structural titanium dioxide ceramic produced by DLP 3D printing. *Ceram Int* 45:23007–23012. <https://doi.org/10.1016/J.CERAMINT.2019.07.346>
 138. Pei E, Loh GH (2018) Technological considerations for 4D printing: an overview. *Prog Addit Manuf* 3:95–107. <https://doi.org/10.1007/S40964-018-0047-1/FIGURES/22>
 139. Srivastava M, Rathee S (2022) Additive manufacturing: recent trends, applications and future outlooks. *Prog Addit Manuf* 7:261–287
 140. Gibson I, Rosen D, Stucker B, Khorasani M (2021) Additive manufacturing technologies. Springer International Publishing, Cham
 141. Henn MC, Mokadam NA (2021) Three-dimensional printing to plan intracardiac operations. *JTCVS Tech* 9:101–108. <https://doi.org/10.1016/j.xjtc.2021.02.050>
 142. Griffith ML, Halloran JW (1996) Freeform fabrication of ceramics via stereolithography. *J Am Ceram Soc* 79:2601–2608. <https://doi.org/10.1111/j.1151-2916.1996.tb09022.x>
 143. Porter NL, Pilliar RM, Grynblas MD (2001) Fabrication of porous calcium polyphosphate implants by solid freeform fabrication: a study of processing parameters and in vitro degradation characteristics. *J Biomed Mater Res* 56:504–515. [https://doi.org/10.1002/1097-4636\(20010915\)56:4%3c504::AID-JBM1122%3e3.0.CO;2-J](https://doi.org/10.1002/1097-4636(20010915)56:4%3c504::AID-JBM1122%3e3.0.CO;2-J)
 144. Choi J-W, Wicker R, Lee S-H et al (2009) Fabrication of 3D biocompatible/biodegradable micro-scaffolds using dynamic mask projection microstereolithography. *J Mater Process Technol* 209:5494–5503. <https://doi.org/10.1016/j.jmatprotec.2009.05.004>
 145. Zarek M, Layani M, Cooperstein I et al (2016) 3D printing of shape memory polymers for flexible electronic devices. *Adv Mater* 28:4449–4454. <https://doi.org/10.1002/ADMA.201503132>
 146. Patel DK, Sakhaei AH, Layani M et al (2017) Highly stretchable and UV curable elastomers for digital light processing based 3D printing. *Adv Mater* 29:1606000. <https://doi.org/10.1002/adma.201606000>
 147. Dong Z, Vuckovac M, Cui W et al (2021) 3D printing of superhydrophobic objects with bulk nanostructure. *Adv Mater*. <https://doi.org/10.1002/adma.202106068>
 148. Dickens PM, Stangroom R, Greul M et al (1995) Conversion of RP models to investment castings. *Rapid Prototyp J* 1:4–11
 149. Kim SY, Shin YS, Jung HD et al (2018) Precision and trueness of dental models manufactured with different 3-dimensional printing techniques. *Am J Orthod Dentofac Orthop* 153:144–153. <https://doi.org/10.1016/J.AJODO.2017.05.025>
 150. Piconi C (2001) Oxide ceramics for biomedical applications. In: *Encyclopedia of materials: science and technology*. Elsevier, pp 6595–6601
 151. Chen F, Zhu H, Wu JM et al (2020) Preparation and biological evaluation of ZrO₂ all-ceramic teeth by DLP technology. *Ceram Int* 46:11268–11274. <https://doi.org/10.1016/J.CERAMINT.2020.01.152>
 152. Schmidleithner C, Malferrari S, Palgrave R et al (2019) Application of high resolution DLP stereolithography for fabrication of tricalcium phosphate scaffolds for bone regeneration. *Biomed Mater* 14:045018. <https://doi.org/10.1088/1748-605X/ab279d>
 153. Liu Z, Liang H, Shi T et al (2019) Additive manufacturing of hydroxyapatite bone scaffolds via digital light processing and in vitro compatibility. *Ceram Int* 45:11079–11086. <https://doi.org/10.1016/j.ceramint.2019.02.195>
 154. Moore DG, Barbera L, Masania K, Studart AR (2020) Three-dimensional printing of multicomponent glasses using phase-separating resins. *Nat Mater* 19:212–217. <https://doi.org/10.1038/s41563-019-0525-y>
 155. Hernández-Rodríguez EM, Acosta-Mora P, Méndez-Ramos J et al (2014) Prospective use of the 3D printing technology for the microstructural engineering of Solid Oxide Fuel Cell components. *Boletín la Soc Española Cerámica y Vidr* 53:213–216. <https://doi.org/10.3989/cyv.252014>
 156. Ozkan B, Sameni F, Bianchi F et al (2022) 3D printing ceramic cores for investment casting of turbine blades, using LCD screen printers: the mixture design and characterisation. *J Eur Ceram Soc* 42:658–671. <https://doi.org/10.1016/j.jeurceramsoc.2021.10.043>
 157. Cao J, Idrees M, Tian G et al (2021) Complex SiC-based structures with high specific strength fabricated by vat photopolymerization and one-step pyrolysis. *Addit Manuf*. <https://doi.org/10.1016/J.ADDMA.2021.102430>
 158. Ratheesh G, Venugopal JR, Chinappan A et al (2017) 3D fabrication of polymeric scaffolds for regenerative therapy. *ACS Biomater Sci Eng* 3:1175–1194. <https://doi.org/10.1021/ACSBOMATERIALS.6B00370>
 159. Kim SH, Hong H, Ajiteru O et al (2021) 3D bioprinted silk fibroin hydrogels for tissue engineering. *Nat Protoc* 2021:1–49. <https://doi.org/10.1038/s41596-021-00622-1>
 160. Lu Y, Mapili G, Suhali G et al (2006) A digital micro-mirror device-based system for the microfabrication of complex, spatially patterned tissue engineering scaffolds. *J Biomed Mater Res Part A* 77A:396–405. <https://doi.org/10.1002/JBM.A.30601>
 161. Zhu W, Ma X, Gou M et al (2016) 3D printing of functional biomaterials for tissue engineering. *Curr Opin Biotechnol* 40:103–112. <https://doi.org/10.1016/j.copbio.2016.03.014>
 162. Advincula RC, Dizon JRC, Caldona EB et al (2021) On the progress of 3D-printed hydrogels for tissue engineering. *MRS Commun* 115(11):539–553. <https://doi.org/10.1557/S43579-021-00069-1>
 163. Traugott NA, Mistry D, Luo C et al (2020) Liquid-crystal-elastomer-based dissipative structures by digital light processing 3D printing. *Adv Mater* 32:2000797. <https://doi.org/10.1002/adma.202000797>
 164. Zhao T, Yu R, Li S et al (2019) Superstretchable and processable silicone elastomers by digital light processing 3D printing. *ACS Appl Mater Interfaces* 11:14391–14398. <https://doi.org/10.1021/ACSAMI.9B03156>
 165. Yunus DE, Sohrabi S, He R et al (2017) Acoustic patterning for 3D embedded electrically conductive wire in stereolithography. *J Micromech Microeng* 27:045016. <https://doi.org/10.1088/1361-6439/AA62B7>
 166. Wu H, Chen P, Yan C et al (2019) Four-dimensional printing of a novel acrylate-based shape memory polymer using digital light processing. *Mater Des* 171:107704. <https://doi.org/10.1016/J.MATDES.2019.107704>
 167. Zhou X, Parida K, Halevi O et al (2020) All 3D printed stretchable piezoelectric nanogenerator for self-powered sensor application. *Sensors (Basel)* 20:1–9. <https://doi.org/10.3390/s20236748>

168. Zhu G, Hou Y, Xiang J et al (2021) Digital light processing 3D printing of healable and recyclable polymers with tailorable mechanical properties. *ACS Appl Mater Interfaces* 13:34954–34961. <https://doi.org/10.1021/ACSAMI.1C08872>
169. Gong H, Beauchamp M, Perry S et al (2015) Optical approach to resin formulation for 3D printed microfluidics. *RSC Adv* 5:106621–106632. <https://doi.org/10.1039/C5RA23855B>
170. Nielsen AV, Beauchamp MJ, Nordin GP, Woolley AT (2020) 3D printed microfluidics. *Annu Rev Anal Chem* 13:45–65. <https://doi.org/10.1146/annurev-anchem-091619-102649>
171. Alam F, Elsherif M, Salih AE, Butt H (2022) 3D printed polymer composite optical fiber for sensing applications. *Addit Manuf* 58:102996. <https://doi.org/10.1016/j.addma.2022.102996>
172. Ali M, Alam F, Fah YF et al (2022) 4D printed thermochromic Fresnel lenses for sensing applications. *Compos Part B Eng* 230:109514. <https://doi.org/10.1016/j.compositesb.2021.109514>
173. Kaur G, Marmur A, Magdassi S (2020) Fabrication of superhydrophobic 3D objects by digital light processing. *Addit Manuf* 36:101669. <https://doi.org/10.1016/J.ADDMA.2020.101669>
174. Andreu A, Su PC, Kim JH et al (2021) 4D printing materials for vat photopolymerization. *Addit Manuf* 44:102024. <https://doi.org/10.1016/J.ADDMA.2021.102024>
175. Saleh Alghamdi S, John S, Roy Choudhury N, Dutta NK (2021) Additive manufacturing of polymer materials: progress, promise and challenges. *Polymers (Basel)* 13:753. <https://doi.org/10.3390/polym13050753>
176. Bhuvanesh Kumar M, Sathiya P (2021) Methods and materials for additive manufacturing: a critical review on advancements and challenges. *Thin-Walled Struct* 159:107228. <https://doi.org/10.1016/j.tws.2020.107228>
177. Vafadar A, Guzzomi F, Rassau A, Hayward K (2021) Advances in metal additive manufacturing: a review of common processes, industrial applications, and current challenges. *Appl Sci* 11:1213. <https://doi.org/10.3390/app11031213>
178. Sugimoto K, Okada N, Kurai S et al (2020) Projection micro stereolithography based 3D printing and its applications. *Int J Extrem Manuf* 2:022004. <https://doi.org/10.1088/2631-7990/AB8D9A>
179. Li Y, Mao Q, Li X et al (2019) High-fidelity and high-efficiency additive manufacturing using tunable pre-curing digital light processing. *Addit Manuf* 30:100889. <https://doi.org/10.1016/j.addma.2019.100889>

Publisher's Note Springer Nature remains neutral with regard to jurisdictional claims in published maps and institutional affiliations.